Studies on interface of pipe joints based on exponential softening bond-slip law under torsional loads

Hong Yuan[1], Jun Han[1], *Ziyong Mo[1], †Lan Zeng[1]

[1]MOE Key Laboratory of Disaster Forecast and Control in Engineering, School of Mechanics and Construction Engineering, Jinan University, China

*Presenting author: moxph33@163.com

†Corresponding author: zenglan@jnu.edu.cn

Abstract

The mechanical behavior and debonding process of pipe joints' interface are the key points for pipe system. In order to better understand and describe the debonding failure of pipe joints subjected to torsional loads for safety design, the theoretical and numerical studies have been conducted. Firstly, based on the exponential softening bond-slip law, the analytical expressions of the interfacial shear stress and the load-displacement relationship at loaded end were obtained. Thus the shear stress propagation and the debonding progress of the whole interface for different bond lengths could be predicted. Secondly, a simplified interface bond-slip law was used by changing the exponential softening law into a bilinear model. The analytical solutions for the simplified model were also obtained. Based on the analytical solutions, the influence of bond length and stiffness on load-displacement curve and ultimate load were discussed. The stress transfer mechanism, the interface crack propagation and the ductility behavior of the joints were further explained.

Keywords: interface; torsion; load-displacement curve; bond-slip law; pipe joints

Introduction

Pipe structures are a very important structural form for energy industry and construction industry. The limitations of the overall system performance usually come from the capacity of pipe joints [1]. Therefore, the pipe joints play the most important role in the overall integrity of most piping systems [2-4].

Based on the mechanics of composite materials and the maximum strain failure criterion, an analytical and experimental study was conducted to investigate the elastic and failure behavior of composite laminated pipe under torsion [5]. Based on the general composite shell theory, Zou et al. [6] studied the stress concentrations at and near the end of the joints as functions of various parameters, such as the overlap length, and thickness of the adhesive layer. Pugno et al. [7] confirmed that the maximum stresses were attained at the ends of the adhesive and that the peak of maximum stress was reached at the end of the stiffer tube and does not tend to zero as the adhesive length approaches infinity. Cheng [8] developed an adhesively bonded smart composite pipe joint system by integrating electromechanical coupling piezoelectric layers with the connection coupler. He et al. [9] studied the failure analysis for thermoplastic composite pipes under combined pure torsion and thermomechanical loading from operational thermal gradients.

A finite element analysis was used to calculate the residual thermal stresses generated by cooling down from the adhesive cure temperature and a nonlinear analysis incorporating the

nonlinear adhesive behavior was performed [10]. Based on a parametric study conducted by 2D and 3D finite element analysis, Hosseinzadeh et al. [11-14] developed a simple method for assessing the behavior of adhesively bonded tubular joints under torsion. A finite difference method was utilized to solve the system of equilibrium equations and it was modeled as a separate 3D elastic body without the uniform stress assumption [15]. Considering individual and combined effect of internal pressure and torsional loadings, Baishya et al. [16] analyzed the failure process of the laminated composite tubes by finite element analysis.

Studies of interfacial mechanical properties are mainly for simple shear model. Yuan et al. [17-19] gave analytical solutions in closed-form of interfacial behavior of adhesive joints. Other researchers made some improvements by considering interfacial normal stress [20-23].

The latest experimental study proposes that exponential softening may appear for interface of some bonded joints [24, 25]. Based on the exponential softening bond-slip law, this paper studies the interface behavior of pipe joints under torsion loads. Closed-form solutions are given.

Interface model of pipe joint

2.1. Interface model

The inner and outer pipe is bonded together by a thin and soft adhesive layer shown in Fig. 1. Here the inner and outer pipe are defined as pipe 1 and 2 respectively. Due to symmetry, only the right half of the pipe joint is considered. We assume that the distance between the left end of pipe 1 and the right end of the pipe 2 is L. For the sake of clarification, the bond length in this paper is denoted by L for only the right half of the pipe joint is considered.

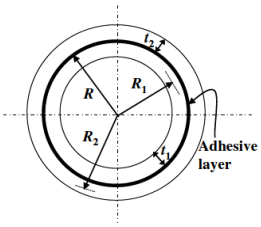

(a) A cross-sectional view

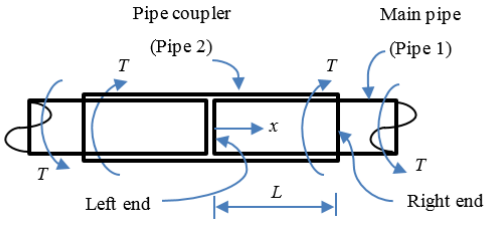

(b) A side view

Fig. 1. Adhesively bonded pipe joint.

Before starting the derivations, the following assumptions can be made for the simplicity of problems:

(1) The adherents are homogeneous and linear elastic;

(2) The adhesive is only exposed to shear forces;

(3) The torsion load carried by the thin and soft adhesive layer is ignored and the external torsion load is assumed to be resisted by the main pipe and coupler pipe;

(4) Local bending effects in the pipe joint under torsion load are neglected.

According to the classical torsion theory, the internal torsion T_1 and T_2 of the pipe and the coupler can be expressed respectively as follows:

$$T_1 = \varphi_1 G_1 J_1 \tag{1}$$

$$T_2 = \varphi_2 G_2 J_2 \tag{2}$$

Where G_1 and G_2, φ_1 and φ_2 are the shear modulus and the rotation angle of pipe 1 and pipe 2 respectively; J_1 and J_2 are the polar moment of inertia of the thin-walled pipe 1 and pipe 2 respectively written as follows:

$$J_1 = 2\pi R_1^3 t_1 \tag{3}$$

$$J_2 = 2\pi R_2^3 t_2 \tag{4}$$

In which, t_1 and t_2 are the thickness of the thin-walled pipe 1 and pipe 2 respectively; R_1 and R_2 are the average radius of pipe 1 and pipe 2 respectively (Figs. 1a).

According to the assumption above, the torsion load carried by the soft and thin adhesive layer is ignored. Thus, the equilibrium between external and internal torsion load in the pipe joint requires:

$$T_1 + T_2 = 0 \tag{5}$$

2.2. Governing equations

If at the given cross-section, the rotations of pipe 1 and pipe 2 are different from each other, a relative rotation occurs accompanied by a circumferential relative displacement at the bond layer. Let's introduce the relative interfacial rotation φ, which equals to the difference of the individual rotation angle of pipe 1 and pipe 2 at the cross-section x as illustrated in Fig. 2. Consider the torsional equilibrium in pipe 1 of an infinitely small section dx as illustrated in Fig. 2:

$$2\pi R\tau R dx = dT_1 \tag{6}$$

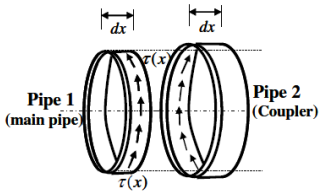

Fig. 2. Equilibrium of the local interfacial shear stresses.

Where τ is the interfacial shear stress along the circumferential direction and R is the distance between the center of the pipe and mid-height of the adhesive layer which can be calculated by:

$$R = \frac{1}{2}\left[\left(R_1 + \frac{t_1}{2}\right) + \left(R_2 - \frac{t_2}{2}\right)\right] \tag{7}$$

Denote this relative slip at the bond layer interface along circumferential direction as δ. This interfacial slip δ can thus be expressed as a function of the relative interfacial rotation φ as follow:

$$\delta = R\varphi = R\varphi_1 - R\varphi_2 \tag{8}$$

By introducing two parameters of local bond strength τ_f and interfacial fracture energy G_f, we have:

$$\frac{d^2\delta}{dx^2} - \frac{2G_f}{\tau_f^2}\lambda^2 f(\delta) = 0 \tag{9}$$

$$\varphi_1' = \frac{\tau_f^2}{2G_f\lambda^2}\frac{2\pi R^2}{G_1 J_1}\frac{d\delta}{dx} \tag{10}$$

where

$$\lambda^2 = 2\pi R^3 \frac{G_1J_1 + G_2J_2}{G_1J_1G_2J_2}\frac{\tau_f^2}{2G_f} \tag{11}$$

Substituting Eq. (10) into (1), the relationship of T_1 and derivative of δ can be obtained:

$$T_1 = 2\pi R^2 \frac{\tau_f^2}{2G_f\lambda^2}\frac{d\delta}{dx} \tag{12}$$

Eq. (9) is the governing differential equation of the adhesive bonded joint in Fig. 2. When the local bond-slip model is found, this equation can be solved.

2.3. Bond-slip model

The exponential bond-slip law can be described as the dashed line in Fig. 3. The interfacial shear stress increases linearly to τ_f at which the value of the slip is denoted by δ_1. It is called an elastic stage. Then interface softening appears and the interfacial shear stress decays exponentially with the interfacial slip. It is called a softening stage. The mathematical expressions of the interfacial bond-slip law in Fig. 3 are:

$$\tau = f(\delta) = \begin{cases} \dfrac{\tau_f}{\delta_1}\delta & (0 \le \delta \le \delta_1) \\ \tau_f e^{-2\alpha^2\left(\frac{\delta}{\delta_1}-1\right)} & (\delta > \delta_1) \end{cases} \tag{13}$$

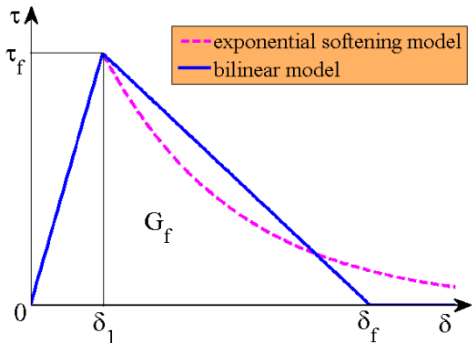

Fig. 3. Bond-slip models.

The bilinear model shown as blue real line in Fig. 3 which features a linear ascending branch followed by a linear descending branch provides a close approximation. It is a simplified model of exponential softening model by letting G_f be equal. According to this model, the bond shear stress increases linearly with the interfacial slip which is the same as exponential model.

Interfacial softening (or micro-cracking) then starts with the shear stress reducing linearly with the interfacial slip. The shear stress reduces to zero when the slip exceeds δ_f, signifying the shear fracture (debonding or macro-cracking) of a local bond element. This bond-slip model shown in Fig. 3 is mathematically described by the following:

$$\tau = f(\delta) = \begin{cases} \dfrac{\tau_f}{\delta_1}\delta & (0 \le \delta \le \delta_1) \\ \dfrac{\tau_f}{\delta_f - \delta_1}(\delta_f - \delta) & (\delta_1 < \delta \le \delta_f) \\ 0 & (\delta > \delta_f) \end{cases} \tag{14}$$

The expression α^2 which is a positive coefficient characterizing the exponential decay could be obtained by letting the interfacial fracture energy G_f in Fig. 3 be equal:

$$\alpha^2 = \frac{\delta_1}{\delta_f - \delta_1} \tag{15}$$

3. Analysis of the debonding process for the exponential model

3.1. Elastic stage

As small loads, there is no interfacial softening or debonding along the interface, so the entire length of the interface is in an elastic stress state. Substituting the relationship of Eq. (13) for the case of $0 \le \delta \le \delta_1$ into (9), the following differential equation is obtained:

$$\delta''(x) - \lambda_1^2 \delta(x) = 0 \quad (0 \le \delta \le \delta_1) \tag{16}$$

where

$$\lambda_1^2 = 2\pi R^3 \frac{G_1 J_1 + G_2 J_2}{G_1 J_1 G_2 J_2} \frac{\tau_f}{\delta_1} \tag{17}$$

And the boundary conditions are:

$$\varphi_1'(0) = 0 \tag{18}$$

$$\varphi_1'(L) = \frac{T}{G_1 J_1} \tag{19}$$

The solution of Eq. (16) for the relative shear displacement as well as the shear stress of the adhesive layer can be written in the form:

$$\delta(x) = \frac{T\delta_1\lambda_1}{2\pi R^2 \tau_f} \frac{\cosh(\lambda_1 x)}{\sinh(\lambda_1 L)} \tag{20}$$

$$\tau(x) = \frac{T\lambda_1}{2\pi R^2} \frac{\cosh(\lambda_1 x)}{\sinh(\lambda_1 L)} \tag{21}$$

The slip at the loaded end (i.e. the value of δ at $x=L$) is defined as the displacement of the bonded joint and is denoted by Δ. According to this definition, the relationship of the load-displacement can be obtained from Eq. (20):

$$T = \frac{2\pi R^2 \tau_f}{\delta_1 \lambda_1} \tanh(\lambda_1 L)\Delta \tag{22}$$

3.2. Elastic-softening stage

As the load increases, the interfacial slip reaches δ_1 at the loaded end and softening appears at $x=L$, thus the whole interface is in an elastic-softening stage. The load T increases as the length of the softening region a increases. Substituting the relationship given in Eq. (13) into (9) gives differential equation (16) for the elastic region and the following equation (23) for the softening region.

$$\delta''(x) - \lambda_2^2 e^{-2\alpha^2 \frac{\delta(x)}{\delta_1}} = 0 \quad (\delta > \delta_1) \tag{23}$$

where

$$\lambda_2^2 = 2\pi R^3 \frac{G_1 J_1 + G_2 J_2}{G_1 J_1 G_2 J_2} \tau_f e^{2\alpha^2} \tag{24}$$

With the boundary conditions of Eqs. (18), (19) and continuous conditions:

$$\delta(L-a) = \delta_1 \tag{25}$$

$$\delta'(x) \text{ is continues at } x = L-a \tag{26}$$

The solution for the elastic region of the interface ($0 \le \delta \le \delta_1$, *i.e.* $0 \le x \le L-a$) is given by:

$$\delta(x) = \frac{\delta_1 \cosh(\lambda_1 x)}{\cosh\left[\lambda_1 (L-a)\right]} \tag{27}$$

$$\tau(x) = \frac{\tau_f \cosh(\lambda_1 x)}{\cosh\left[\lambda_1 (L-a)\right]} \tag{28}$$

and the solution for the softening region of the interface ($\delta > \delta_1$, *i.e.* $L-a \le x \le L$) is shown as follows:

$$\delta(x) = \frac{1}{n}\ln\left(\frac{2m}{nc_1}\right) + \frac{2}{n}\ln\left\{\cosh\left[\frac{n}{2}\sqrt{c_1}(x-c_2)\right]\right\} \tag{29}$$

$$\tau(x) = \tau_f e^{-2\alpha^2\left[\frac{\delta(x)}{\delta_1}-1\right]} \tag{30}$$

where

$$m = \lambda_2^2 \tag{31}$$

$$n = \frac{2\alpha^2}{\delta_1} \tag{32}$$

Based on the conditions Eqs. (25) and (26), the constants c_1 and c_2 can be obtained:

$$c_1 = \left\{\delta_1 \lambda_1 \tanh\left[\lambda_1 (L-a)\right]\right\}^2 + \frac{2m}{n} e^{-n\delta_1} \tag{33}$$

$$c_2 = L - a - \frac{2}{n\sqrt{c_1}} \operatorname{arccosh}\left(\sqrt{\frac{nc_1}{2m} e^{n\delta_1}}\right) \tag{34}$$

The expression of slip at loaded end can be obtained from Eq. (29) when $x=L$:

$$\Delta = \delta(L) = \frac{1}{n} \ln\left(\frac{2m}{nc_1}\right) + \frac{2}{n} \ln\left\{\cosh\left[\frac{n}{2}\sqrt{c_1}(L - c_2)\right]\right\} \tag{35}$$

Substituting Eqs. (19) and (29) into (10) yields:

$$T = \frac{2\pi R^2 \tau_f}{\delta_f \lambda^2} \sqrt{-\frac{2m}{n} e^{-n\Delta} + c_1} \tag{36}$$

For exponential model, the expression of T above can be rewritten as:

$$T = \frac{2\pi R^2 \tau_f}{\delta_f \lambda^2} \sqrt{c_1} \tanh\left[\frac{n}{2}\sqrt{c_1}\left(L - c_2\right)\right] \tag{37}$$

T reaches its maximum when L is large enough so Eqs. (37) and (33) converge to:

$$T_u = \frac{2\pi R^2 \tau_f}{\delta_f \lambda^2} \sqrt{c_1} \tag{38}$$

where

$$c_1 = \left(\delta_1 \lambda_1\right)^2 + \frac{2m}{n} e^{-n\delta_1} \tag{39}$$

The length of the interface that is mobilized to resist the applied load is generally referred to as the effective bond length. This effective bond length is defined here as the bond length over which the shear stresses offer a total resistance which is at least 97% of the applied load for a joint with an infinite bond length. The effective bond length when T_u is reached can be obtained from Eqs. (34) and (37)-(39) to give:

$$l_e = a_e + \frac{2}{\lambda_1} \tag{40}$$

where

$$a_e = \frac{4}{n\sqrt{c_1}} - \frac{2}{n\sqrt{c_1}} \operatorname{arccosh}\left(\sqrt{\frac{nc_1}{2m} e^{n\delta_1}}\right) \tag{41}$$

3.3. Softening stage

As the load increases, the peaks of shear stress move to the unloaded end (x=0). When the interfacial slip at x=0 reaches δ_1, the whole interface enters into softening zone. This stage is governed by Eq. (23) with boundary conditions (18) and (19).

Based on the boundary conditions, the solution for the interfacial slip and the shear stress of the adhesive layer can be written in the form:

$$\delta(x)=\frac{1}{n}\ln\left(\frac{2m}{nc_3}\right)+\frac{2}{n}\ln\left\{\cosh\left[\frac{n}{2}\sqrt{c_3}(x-c_4)\right]\right\} \tag{42}$$

$$\tau(x)=\tau_f e^{-2\alpha^2\left[\frac{\delta(x)}{\delta_1}-1\right]} \tag{43}$$

where the constants c_3 and c_4 are shown as follows:

$$c_3\tanh^2\left[\frac{n\sqrt{c_3}}{2}(L-c_4)\right]=\left(\frac{T\delta_f\lambda^2}{2\pi R^2\tau_f}\right)^2 \tag{44}$$

$$c_4=0 \tag{45}$$

Substituting Eqs. (19) and (42) into (10) yields:

$$T=\frac{2\pi R^2\tau_f}{\delta_f\lambda^2}\sqrt{-\frac{2m}{n}e^{-n\Delta}+c_3} \tag{46}$$

The expression of slip at loaded end can be obtained from Eq. (42) when $x=L$:

$$\Delta=\frac{1}{n}\ln\left(\frac{2m}{nc_3}\right)+\frac{2}{n}\ln\left\{\cosh\left[\frac{n}{2}\sqrt{c_3}(L-c_4)\right]\right\} \tag{47}$$

4. Analysis of the debonding process for the bilinear model

4.1. Elastic stage

The elastic stage is the same as the elastic stage in 3.1, thus the expressions of the interfacial slip, shear stress and the relationship of the load-displacement are the same.

4.2. Elastic-softening stage

As the load increases, softening commences at the loaded end once the shear stress reaches τ_f at $x=L$. The load T increases as the softening length a increases. Substituting the relationship given in Eq. (14) into (9) gives Eqs. (16) for the elastic region and (48) for the softening region.

$$\delta''(x)-\lambda_3^2\left[\delta_f-\delta(x)\right]=0 \quad (\delta_1<\delta\le\delta_f) \tag{48}$$

where

$$\lambda_3^2=2\pi R^3\frac{G_1J_1+G_2J_2}{G_1J_1G_2J_2}\frac{\tau_f}{\delta_f-\delta_1} \tag{49}$$

With the same boundary conditions (18), (19) and continuous conditions (25), (26) used in 3.2. The solution for the elastic region of the interface ($0\le\delta\le\delta_1$, *i.e.* $0\le x\le L-a$) is the same as in 3.2. And the solution for the softening region of the interface ($\delta_1<\delta\le\delta_f$, *i.e.* $L-a\le x\le L$) is given by:

$$\delta(x)=(\delta_f-\delta_1)\left\{\frac{\lambda_3}{\lambda_1}\tanh\left[\lambda_1(L-a)\right]\sin\left[\lambda_3(x-L+a)\right]-\cos\left[\lambda_3(x-L+a)\right]+\frac{\delta_f}{\delta_f-\delta_1}\right\} \tag{50}$$

$$\tau(x)=-\tau_f\left\{\frac{\lambda_3}{\lambda_1}\tanh\left[\lambda_1(L-a)\right]\sin\left[\lambda_3(x-L+a)\right]-\cos\left[\lambda_3(x-L+a)\right]\right\} \tag{51}$$

Substituting Eqs. (19) and (50) into (10) yields:

$$T = \frac{2\pi R^2 \tau_f}{\lambda_3}\left\{\frac{\lambda_3}{\lambda_1}\tanh\left[\lambda_1(L-a)\right]\cos(\lambda_3 a)+\sin(\lambda_3 a)\right\} \tag{52}$$

The expression of the slip at the loaded end could be got from Eq. (50) when $x=L$:

$$\Delta = (\delta_f - \delta_1)\left\{\frac{\lambda_3}{\lambda_1}\tanh\left[\lambda_1(L-a)\right]\sin(\lambda_3 a)-\cos(\lambda_3 a)+\frac{\delta_f}{\delta_f-\delta_1}\right\} \tag{53}$$

During this stage, the load-displacement curve could be drawn from Eqs. (52) and (53). When the interfacial slip increases to δ_f at $x=L$ and the slip at $x=0$ less than δ_1, we can get $L>\frac{\pi}{2\lambda_3}$ and the interface enters into elastic-softening-debonding stage. When the slip at $x=0$ reaches δ_1 and the slip at loaded end less than δ_f, we can get $L<\frac{\pi}{2\lambda_3}$ and the interface enters into softening stage. Therefore, there exists a critical bond length to distinguish the coming failure process:

$$L_{cr} = \frac{\pi}{2\lambda_3} \tag{54}$$

For bilinear model, T reaches its maximum when the derivative of Eq. (52) with respect to a equal zero. Therefore, a at the ultimate load can be found from the following relationship:

$$\tanh\left[\lambda_1(L-a)\right] = \frac{\lambda_3}{\lambda_1}\tan(\lambda_3 a) \tag{55}$$

Substituting Eq. (55) into (52) yields:

$$T = \frac{2\pi R^2 \tau_f}{\lambda_3}\frac{\delta_f}{\delta_f-\delta_1}\sin(\lambda_3 a) \tag{56}$$

It can be shown from Eq. (55) that for large values of L Eq. (56) converges to:

$$T_u = \frac{2\pi R^2 \tau_f}{\lambda} \tag{57}$$

Based on same definition of effective bond length in 3.2 and considering that $\tanh(2)\approx 0.97$, the effective bond length when T_u is reached can be obtained from Eqs. (55)-(57) to give:

$$l_e = a_e + \frac{1}{2\lambda_1}\ln\left[\frac{\lambda_1+\lambda_3\tan(\lambda_3 a_e)}{\lambda_1-\lambda_3\tan(\lambda_3 a_e)}\right] \tag{58}$$

where

$$a_e = \frac{1}{\lambda_3}\arcsin\left[0.97\sqrt{\frac{\delta_f-\delta_1}{\delta_f}}\right] \tag{59}$$

4.3. $L>L_{cr}$

4.3.1. Elastic-softening-debonding stage

If $L>L_{cr}$, as the load increases the interfacial slip at loaded end reaches δ_f and debonding (or

macro-cracking or fracture) commences and propagates along the interface. At the initiation of debonding $\Delta=\delta_f$ and by making use of this condition, the corresponding value of a, denoted by a_d, can be obtained from Eq. (53) as:

$$\frac{\lambda_3}{\lambda_1}\tanh\left[\lambda_1(L-a_d)\right]\sin(\lambda_3 a_d)-\cos(\lambda_3 a_d)=0 \tag{60}$$

As debonding propagates, the peak shear stress moves towards the unloaded end. Assuming that the debonded length of the interface starting at the loaded end is d, Eqs. (27), (28), (50) and (51) are still valid if replacing L by L-d. Therefore, the load-displacement relationship can be written as:

$$T=\frac{2\pi R^2\tau_f}{\lambda_3}\left\{\frac{\lambda_3}{\lambda_1}\tanh\left[\lambda_1(L-d-a)\right]\cos(\lambda_3 a)+\sin(\lambda_3 a)\right\} \tag{61}$$

$$\Delta=\delta_f+\frac{\delta_f T\lambda^2}{2\pi R^2\tau_f}d \tag{62}$$

As the interfacial shear stress at $x=L$-d is zero, the following relationship can be obtained:

$$\frac{\lambda_3}{\lambda_1}\tanh\left[\lambda_1(L-d-a)\right]\sin(\lambda_3 a)-\cos(\lambda_3 a)=0 \tag{63}$$

Substituting Eq. (63) into (61) yields the following simplified form:

$$T=\frac{2\pi R^2\tau_f}{\lambda_3}\frac{1}{\sin(\lambda_3 a)} \tag{64}$$

At the end of this stage, the softening-debonding stage starts when L-$d=a_u$. Substituting the relation into Eq. (63) yields:

$$a_u=\frac{\pi}{2\lambda_3} \tag{65}$$

Moreover, Eq. (64) can be written as:

$$T=\frac{2\pi R^2\tau_f}{\lambda_3} \tag{66}$$

4.3.2. Softening-debonding stage

This stage is governed by Eq. (48) with boundary conditions of Eq. (18) and:

$$\varphi_1'(a)=\frac{T}{G_1 J_1} \tag{67}$$

$$\delta(a)=\delta_f \tag{68}$$

The following solution can thus be found:

$$a=\frac{\pi}{2\lambda_3}=a_u \tag{69}$$

$$\delta(x)=\delta_f-\frac{\delta_f T\lambda^2}{2\pi R^2\tau_f\lambda_3}\cos(\lambda_3 x)\quad(0\le x\le a_u) \tag{70}$$

$$\tau(x)=\frac{\lambda_3 T}{2\pi R^2\cos(\lambda_3 x)}\quad(0\le x\le a_u) \tag{71}$$

It can be concluded from Eq. (69) that the length of softening zone remains constant during this stage. The load-displacement relationship can be simply obtained by displacement superposition along the bonded joint:

$$\Delta=\delta_f+\frac{\delta_f T\lambda^2}{2\pi R^2\tau_f}(L-a_u) \tag{72}$$

4.4. L<L$_{cr}$

4.4.1. Softening stage

As the load increases, the peaks of shear stress move to the unloaded end. When the interfacial slip at x=0 reaches δ_1, the whole interface enters into softening zone. This stage is governed by Eq. (48) with boundary conditions of Eqs. (18) and (19). The following solution can be obtained:

$$\delta(x)=\delta_f-\frac{T\lambda^2\delta_f\cos(\lambda_3 x)}{2\pi R^2\tau_f\lambda_3\sin(\lambda_3 L)} \tag{73}$$

$$\tau(x)=\frac{T\lambda_3\cos(\lambda_3 x)}{2\pi R^2\sin(\lambda_3 L)} \tag{74}$$

The expression of the slip at the loaded end could be obtained from Eq. (73) when x=L:

$$\Delta=\delta_f-\frac{T\lambda^2\delta_f}{2\pi R^2\tau_f\lambda_3}\cot(\lambda_3 L) \tag{75}$$

5. Numerical simulations

The typical inner diameter and thickness are assumed to be 290 and 10 mm for the main pipe, respectively. And the inner diameter and thickness of the coupler are assumed to be 311 and 15 mm, respectively. The shear moduli G_1 and G_2 are assumed to be 28 GPa for both main pipe and coupler. The parameters for interfacial bond-slip laws are identified as: τ_f=7.2 MPa, δ_1=0.034 mm, δ_f=0.16 mm.

According to the material properties and geometry parameters given above, the critical bond length for bilinear model can be calculated as L_{cr}=85 mm. Therefore, bond length of 50 and 100 mm are chosen.

5.1. Load-displacement curves

5.1.1. Load-displacement curves for exponential model

The load-displacement curve for exponential model is shown in Fig. 4. OA, AB and BC are elastic, elastic-softening and softening stages, respectively.

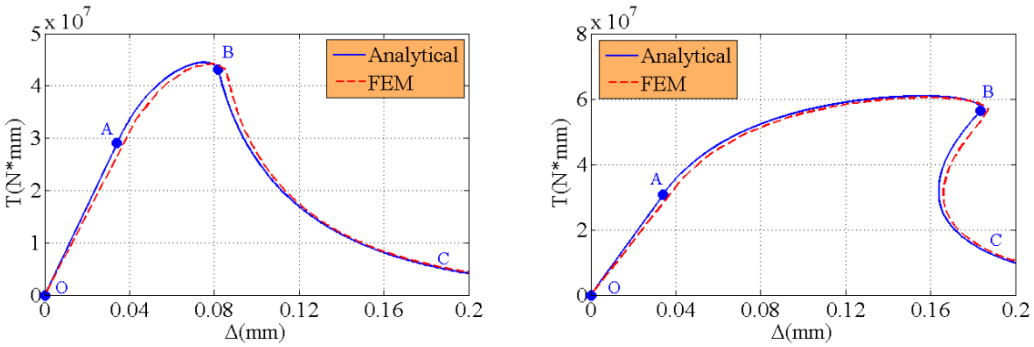

(a) L=50 mm (b) L=100 mm

Fig. 4. Load-displacement curves for exponential model.

5.1.2. Load-displacement curves for bilinear model

When the bond length is shorter than L_{cr}, take L=50 mm and the load-displacement curve is shown in Fig. 5(a). OA, AB and BC are elastic, elastic-softening and softening stages, respectively. When the bond length is longer than L_{cr}, take L=100 mm and the load-displacement curve is shown in Fig. 5(b). OA, AB, BC and CD are elastic, elastic-softening, elastic-softening-debonding and softening-debonding stages, respectively. The FEA results by using commercial software ABAQUS are also given for comparison in Fig. 4 and Fig. 5. In ABAQUS modelling, C3D8R, which is an 8-node linear brick element with reduced integration scheme, is used for both main pipe and coupler. And for adhesive layer, COH3D8, which is an 8-node three-dimensional cohesive element, is used.

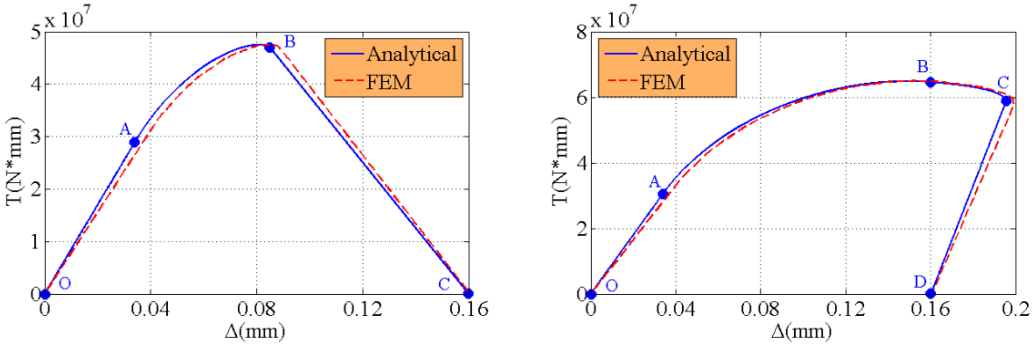

(a) L=50 mm (b) L=100 mm

Fig. 5. Load-displacement curves for bilinear model.

5.2. Shear stress distribution

The shear stress distribution for exponential model is shown in Fig. 6. When the load is small, the interfacial shear stress at loaded end is less than peak stress and the interface is in an elastic stage. When the interfacial shear stress reaches peak stress at loaded end, the interface enters into elastic-softening stage. As load increases, the peak stress moves from loaded end to unloaded end and the length of softening zone increases. When the interfacial shear stress at unloaded end reaches peak stress, the interface enters into softening stage.

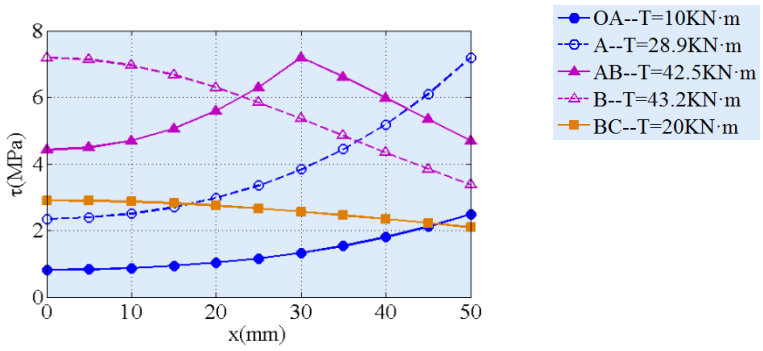

(a) L=50 mm

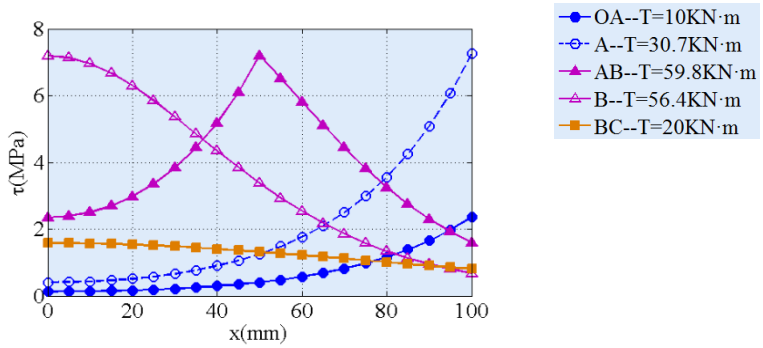

(b) L=100 mm

Fig. 6. Shear stress distribution for exponential model.

The shear stress distribution of L=50 mm and L=100 mm for bilinear model are shown in Fig. 7(a) and (b) respectively. When the load is small, the interfacial shear stress at loaded end is less than peak stress and the interface is an in elastic stage. When the interfacial shear stress reaches peak stress at loaded end, the interface enters into elastic-softening stage. As load increases, the peak stress moves from loaded end to unloaded end and the length of softening zone increases. When the interfacial shear stress at unloaded end reaches peak stress while $\Delta<\delta_f$, the interface enters into softening stage shown as in Fig. 7(a). When $\Delta=\delta_f$ and the interfacial shear stress at unloaded end is less than peak stress, then the interface enters into elastic-softening-debonding stage shown as in Fig. 7(b). The length of debonding zone increases as the peak stress moves to unloaded end. When the interfacial shear stress at unloaded end reaches peak stress, the interface enters into softening-debonding stage.

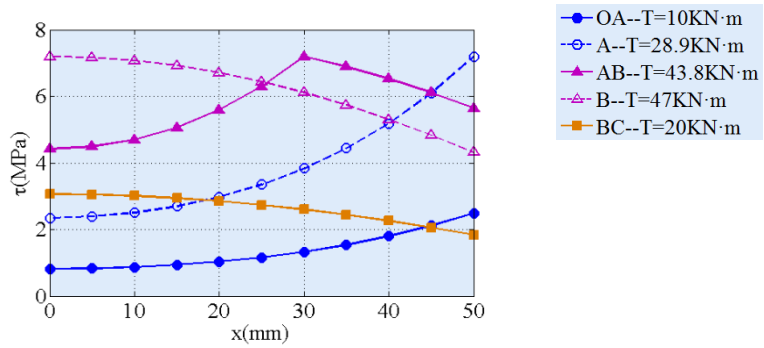

(a) L=50 mm

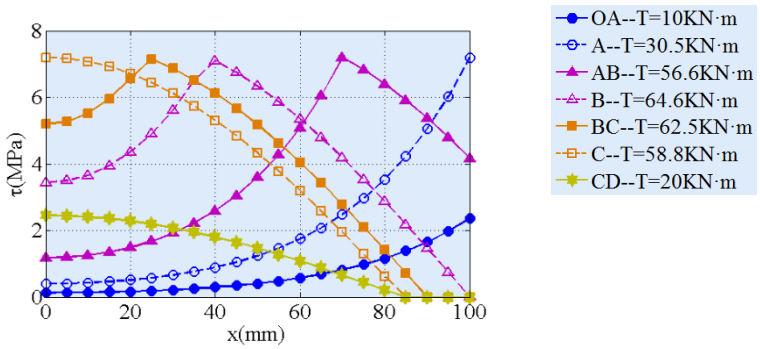

(b) L=100 mm

Fig. 7. Shear stress distribution for bilinear model.

5.3. Parametric study

Fig. 8(a) shows the influence of bond lengths on the load-displacement curves for bilinear model. From the figure, the significant influence for bond length on the curves could be observed. In the range of the effective bond length, as the bond length increases, not only the interface failure processes change but also the ultimate load and interfacial slip. Specifically, the increase of the bond length can increase damage ductility. However, when the bond length reaches a certain length (effective bond length), the ultimate load will hardly change. Fig. 8(b) shows the influence of bond lengths on the load-displacement curves for exponential model. From the figure we know that the ultimate load increases as the bond length increases. But the failure processes are all the same. The increase of the bond length can also increase damage ductility.

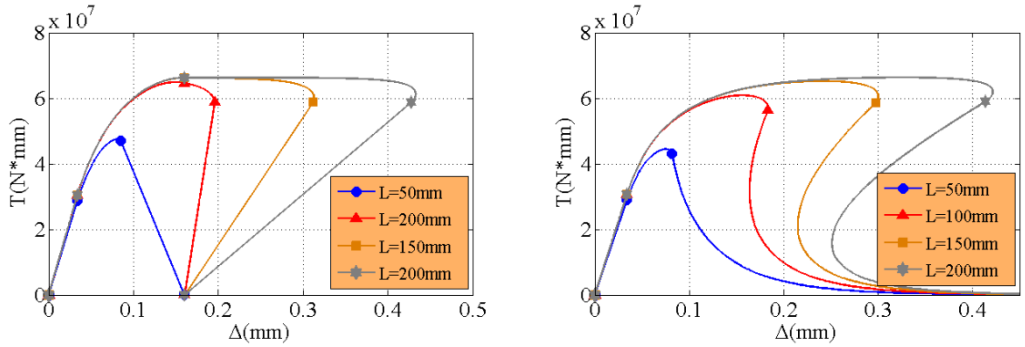

(a) bilinear model (b) exponential model

Fig. 8. Load-displacement curves for different bond lengths.

Fig. 9 shows the comparison of the load-displacement curves between the two models for different bond lengths. The load-displacement curves are different when a softening area exists. In addition, since there is no debonding initiation in the exponential model, the displacement can increase unlimitedly, with this being different from bilinear model in which the slip would approach δ_f. From the figures, the load increases faster in the bilinear model as the bond lengths increases. However, when the bond length is long, the ultimate loads between the two models seem no more difference.

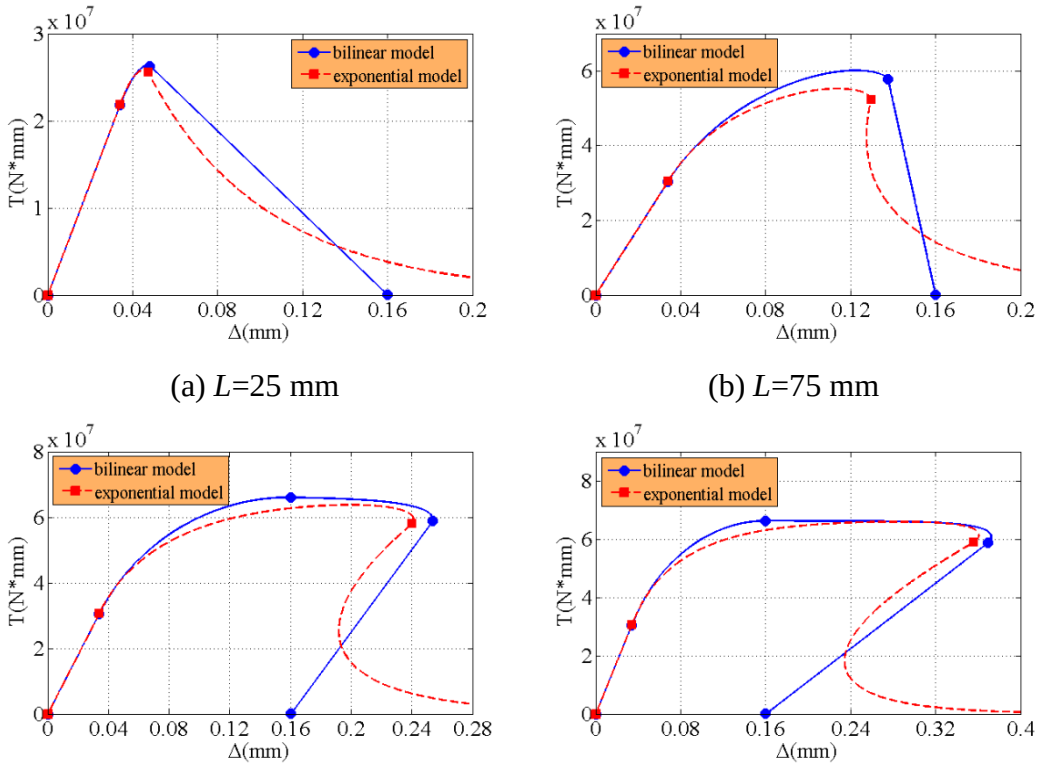

(a) L=25 mm (b) L=75 mm

(c) L=125 mm (d) L=175 mm

Fig. 9. Comparison of the load-displacement curves of the two models for different bond lengths.

Fig. 10 shows the load-displacement curves for different ratios of torsion stiffness ($\beta = G_2J_2/G_1J_1$). From the figures we can see that as the ratio increases, the ultimate load increases but the slip decreases, namely the ductility reduces.

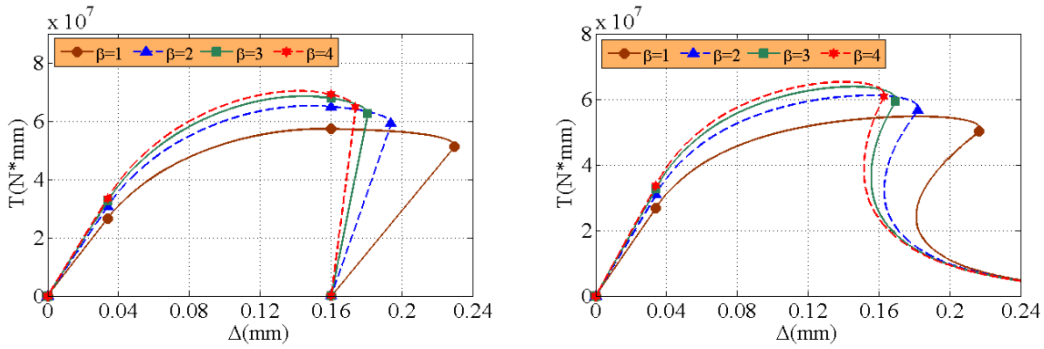

(a) bilinear model (b) exponential model

Fig. 10. Load-displacement curves for different ratios of torsion stiffness.

Fig. 11 shows the relationship between effective bond length and ratio of torsion stiffness. From the figure we can see that a stiffer coupler leads to a longer effective bond length. But as the ratio getting larger, the effective bond length increases not obviously. As the ratio increases, the effective bond length of two models have the similar trend, but the effective bond length of exponential model is longer than that of bilinear model.

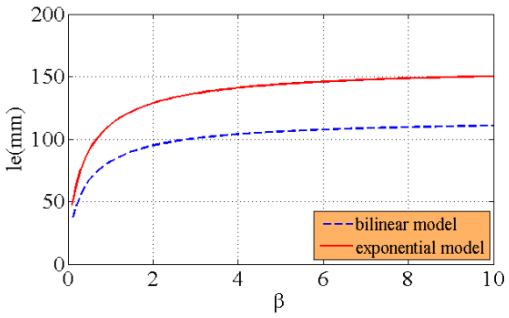

Fig. 11. Effect of ratio of torsion stiffness on the effective bond length.

Through the numerical computation, the ultimate load of exponential and bilinear models for different bond lengths could be obtained. Fig. 12 shows the ultimate load for different bond lengths. From the figure we can see that for bilinear model, when the bond length is short, the ultimate load increases significantly with the bond length. When the bond length is long, the ultimate load stays essentially unchanged. For the exponential model, when the bond length is short, the trend is similar to the bilinear model, but the ultimate load is relatively smaller. Both models have the same ultimate load when the bond length is relatively long.

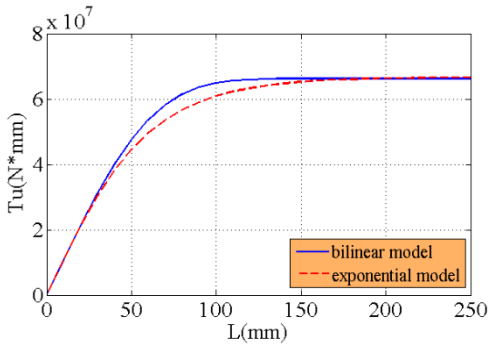

Fig. 12. The ultimate load of two models for different bond lengths.

Conclusions

On the basis of fully understanding the mechanical behavior of the pipe joints' interface, this paper gives a further understanding of the key factors of interfacial debonding. By modifying the torsion stiffness, the present models may be further extended to orthotropic materials, such as fiber-reinforced composite pipe joints. Based on the derivations in the current study, some important conclusions are summarized as follows:

(1) Through the nonlinear fracture mechanics, the analytical expressions of the interfacial shear stress and the load-displacement relationship at loaded end of pipe joints under torsion loads could be got. Thus the shear stress propagation and the debonding progress of the whole interface for different bond lengths could be predicted.

(2) The influences of different bond length on the load-displacement curve and the ultimate load are studied through the analytical solutions. The stress transfer mechanism, the interface crack propagation and the ductility behavior of the joints could be explained.

Acknowledgements

The authors gratefully acknowledge the financial support provided by the Guangdong Basic

and Applied Basic Research Foundation (No. 2020A1515010095) and the Young Science and Technology Talent Support Project of Guangzhou Association for Science and Technology (No. X20210201066).

References

[1] Lv Y., Liu C.F., Huang X., Chen Y., Chouw N. (2021) Experimental and Finite-Element Studies of Buried Pipes Connected by a Bellow Joint under Cyclic Shear Loading, *Journal of Pipeline Systems Engineering and Practice* **12**.
[2] Ouyang Z.Y., Li G.Q. (2009) Interfacial debonding of pipe joints under torsion loads: a model for arbitrary nonlinear cohesive laws, *International Journal of Fracture* **155**, 19-31.
[3] Ouyang Z.Y., Li G.Q. (2009) Cohesive zone model based analytical solutions for adhesively bonded pipe joints under torsional loading, *International Journal of Solids and Structures* **46**, 1205-1217.
[4] Fame C.M., Correia J.R., Ghafoori E., Wu C. (2021) Damage tolerance of adhesively bonded pultruded GFRP double-strap joints, *Composite Structures* **263**,113625.
[5] Zhao Y., Pang S.S. (1995) Stress-strain and failure analyses of composite pipe under torsion, *Journal of Pressure Vessel Technology-Transactions of the Asme* **117**, 273-278.
[6] Zou G.P., Taheri F. (2006) Stress analysis of adhesively bonded sandwich pipe joints subjected to torsional loading, *International Journal of Solids and Structures* **43**, 5953-5968.
[7] Pugno N., Surace G. (2001) Tubular bonded joint under torsion: Theoretical analysis and optimization for uniform torsional strength, *Journal of Strain Analysis for Engineering Design* **36**, 17-24.
[8] Cheng J.Q., Li G.Q. (2008) Stress analysis of a smart composite pipe joint integrated with piezoelectric composite layers under torsion loading, *International Journal of Solids and Structures* **45**, 1153-1178.
[9] He Y., Vaz M.A., Caire M. (2021) Stress and failure analyses of thermoplastic composite pipes subjected to torsion and thermomechanical loading, *Marine Structures* **79**.
[10] Oh J.H. (2007) Strength prediction of tubular composite adhesive joints under torsion, *Composites Science and Technology* **67**, 1340-1347.
[11] Hosseinzadeh R., Taheri F. (2009) Non-linear investigation of overlap length effect on torsional capacity of tubular adhesively bonded joints, *Composite Structures* **91**, 186-195.
[12] Hosseinzadeh R., Cheraghi N., Taheri F. (2006) An engineering approach for design and analysis of metallic pipe joints under torsion by the finite element method. *Journal of Strain Analysis for Engineering Design* **41**, 443-452.
[13] Hosseinzadeh R., Shahin K.,Taheri F. (2007) A simple approach for characterizing the performance of metallic tubular adhesively-bonded joints under torsion loading, *Journal of Adhesion Science and Technology* **21**, 1613-1631.
[14] Esmaeel R.A., Taheri F. (2011) Influence of adherend's delamination on the response of single lap and socket tubular adhesively bonded joints subjected to torsion, *Composite Structures* **93**, 1765-1774.
[15] Xu W., Li G.Q. (2010) Finite difference three-dimensional solution of stresses in adhesively bonded composite tubular joint subjected to torsion, *International Journal of Adhesion and Adhesives* **30**, 191-199.
[16] Baishya N., Das R.R., Panigrahi S.K. (2017) Failure analysis of adhesively bonded tubular joints of laminated FRP composites subjected to combined internal pressure and torsional loading, *Journal of Adhesion Science and Technology* **31**, 2139-2163.
[17] Yuan H., Wu Z.S.,Yoshizawa H. (2001) Theoretical solutions on interfacial stress transfer of externally bonded steel/composite laminates, *Doboku Gakkai Ronbunshu* **2001**, 27-39.
[18] Wu Z.S., Yuan H., Niu H.D. (2002) Stress transfer and fracture propagation in different kinds of adhesive joints, *Journal of Engineering Mechanics* **128**, 562-573.
[19] Yuan H., Teng J.G., Seracino R., Wu Z.S., Yao J. (2004) Full-range behavior of FRP-to-concrete bonded joints, Engineering Structures **26**, 553-565.
[20] Caggiano A., Martinelli E.,Faella C. (2012) A fully-analytical approach for modelling the response of FRP plates bonded to a brittle substrate, International Journal of Solids and Structures **49**, 2291-2300.
[21] Chen F.L., Qiao P.Z. (2009) Debonding analysis of FRP-concrete interface between two balanced adjacent flexural cracks in plated beams, International Journal of Solids and Structures **46**, 2618-2628.
[22] Lorenzis L.D., Zavarise G.: Cohesive zone modeling of interfacial stresses in plated beams. Int. J. Solids Struct.**46**, 4181-4191 (2009)
[23] Wang J.L. (2007) Cohesive zone model of FRP-concrete interface debonding under mixed-mode loading, International Journal of Solids and Structures **44**, 6551-6568.
[24] Woo, S., Lee, Y. (2010) Experimental study on interfacial behavior of CFRP-bonded concrete, KSCE Journal of Civil Engineering **14**, 385-393.
[25] Yuan H., Lu X.S., Hui D., Feo L. (2012) Studies on FRP-concrete interface with hardening and softening bond-slip law, Composite Structures **94**, 3781-3792.